

Nanoporous Au Formation on Au Substrates via High Voltage Electrolysis**

Evelyn Artmann,^[a] Lukas Forschner,^[a] Konstantin M. Schüttler,^[b] Mohammad Al-Shakran,^[a] Timo Jacob,^[a] and Albert K. Engstfeld^{*[a]}

Nanoporous Au (NPG) films have promising properties, making them suitable for various applications in (electro)catalysis or (bio)sensing. Tuning the structural properties, such as the pore size or the surface-to-volume ratio, often requires complex starting materials such as alloys, multiple synthesis steps, lengthy preparation procedures or a combination of these factors. Here we present an approach that circumvents these difficulties, enabling for a rapid and controlled preparation of NPG films starting from a bare Au electrode. In a first approach a Au oxide film is prepared by high voltage (HV) electrolysis in a KOH solution, which is then reduced either electrochemically or in the presence of H₂O₂. The resulting NPG structures and

their electrochemically active surface areas strongly depend on the reduction procedure, the concentration and temperature of the H₂O₂-containing KOH solution, as well as the applied voltage and temperature during HV electrolysis. Secondly, the NPG film can be prepared directly by applying voltages that result in anodic contact glow discharge electrolysis (aCGDE). By carefully adjusting the corresponding parameters, the surface area of the final NPG film can be specifically controlled. The structural properties of the electrodes are investigated by means of XPS, SEM and electrochemical methods.

Introduction

Nanoporous metals show distinct physico-chemical properties that often differ from those of the bulk materials.^[1–4] These materials typically have pores in the range of 50 to 200 nm interconnected with ligaments of the bulk material. A rather intensively studied systems during the last years is nanoporous Au (NPG), for its possible application as, i.e., (bio)sensor,^[1,5–9] in biomedicine,^[9] as actuator,^[10] heterogeneous catalyst material,^[8,11–13] electrocatalyst,^[1,2,14–18] or material in battery systems.^[1,2]

A large number of approaches exist to prepare NPG, either free standing or on a support material.^[1,2,7,8,19] The most common method discussed to synthesize nanoporous structures in general is dealloying, which is not limited to Au but is

successfully employed for example to create nanoporous Ni (Raney-Ni).^[2,20] Within this approach, an alloy is used as precursor, which can for example be fabricated by electrodeposition of one metal on another followed by alloying both elements. In a subsequent electrochemical dealloying step, the less noble metal is dissolved (electro)chemically and a nanoporous structure of the more noble metal remains.^[11,21] This method is, however, mostly limited to noble metals.^[2] To prepare NPG, the precursor alloy usually consists of a mixture of Ag and Au.^[6,13,15,16,22,23]

Another frequently used method is the reduction of precursor molecules such as metal salts, e.g., HAuCl₄, in solution.^[24] The reduction of the precursor molecules can, for example, be achieved by igniting a plasma above a liquid,^[25–27] or by using another molecule that acts as a reducing agent.^[28,29] By combining different preparation methods, not only NPG films but also nanoporous Au nanoparticles can be produced.^[30]

NPG films can also be prepared by anodizing a Au substrate in aqueous solutions at potentials in the oxygen evolution region (for example 2.0 V vs. Ag/AgCl) and subsequent electrochemical reduction.^[31,32] This approach bears the advantage that no additional chemicals or multimetallic precursors have to be used. Other groups also report on combining electrodeposition with subsequent anodization.^[33] Overall, most of these common processes for producing nanoporous substrates are relatively complex, time-consuming, and require different, potentially harmful chemicals, which can also lead to the incorporation of impurities in the nanoporous film (in case of alloy precursors or salts). Impurities in particular can be problematic in further (electro)catalytic studies, where trace impurities can have a significant impact on the reaction rates such as for the CO

[a] E. Artmann, L. Forschner, Dr. M. Al-Shakran, Prof. Dr. T. Jacob, Dr. A. K. Engstfeld
Institute of Electrochemistry
Ulm University
D-89081 Ulm, Germany
+49 (0)731 25401
+49 (0)731 25409
E-mail: albert.engstfeld@uni-ulm.de

[b] K. M. Schüttler
Institute of Surface Chemistry and Catalysis
Ulm University
D-89081 Ulm, Germany

[**] A previous version of this manuscript has been deposited on a preprint server (DOI: <https://doi.org/10.26434/chemrxiv-2022-mx2qd>).

 Supporting information for this article is available on the WWW under <https://doi.org/10.1002/cphc.202200645>

 © 2022 The Authors. ChemPhysChem published by Wiley-VCH GmbH. This is an open access article under the terms of the Creative Commons Attribution Non-Commercial License, which permits use, distribution and reproduction in any medium, provided the original work is properly cited and is not used for commercial purposes.

oxidation.^[34,35] To scale up material production it is necessary that the production process is cheap, fast, reliable and preferentially does not pose any environmental hazards.

Recently, we demonstrated that NPG films can be prepared by anodization of a Au electrode in aqueous alkaline electrolyte at high voltages (between 100 and 540 V) leading to the formation of a Au oxide film, which upon subsequent electrochemical reduction turns into a NPG film.^[36] NPG films with similar structures were also obtained by keeping the Au oxide after electrolysis in the electrolysis solution. We suggested that the Au oxide is reduced by H₂O₂ which forms during anodic contact glow discharge electrolysis (aCGDE).^[37–40] Our results also indicate that H₂O₂ might also form at lower voltages (still in the range of a few 100 V) in the normal electrolysis region, as suggested previously.^[41] This approach allows preparing samples within a few minutes. In addition, this method is also comparably environmental friendly since an alkaline KOH solution is the only chemical used in the preparation process.

In this work we systematically investigate the formation of NPG on bare Au wire and sheet electrodes. The experimental approach is based on our previous study, whereby a Au electrode is oxidized during electrolysis at high voltage (HV) in 0.01 M KOH and subsequently reduced either electrochemically or in a H₂O₂-containing 0.01 M KOH solution. The conclusions on the composition of the electrodes after this procedure by electrochemical measurements in the previous work are here confirmed by XPS measurements. Furthermore, with cross sectional SEM analyses we show that the Au oxide, obtained after HV electrolysis, as well as the NPG film, obtained after reducing the Au oxide, forms a several micrometer thick layer. In order to tune the NPG film, we systematically explore the possibility to reduce the Au oxide with H₂O₂ solutions with different concentration and temperature. The final NPG structures are compared to those obtained by electrochemical reduction. We also demonstrate that the thickness (or surface area) of the NPG film can be controlled by varying the electrolysis time, the electrolyte temperature, and the voltage applied during electrolysis. The structural properties are investigated primarily by SEM imaging and electrochemical measurements.

Results and Discussion

The results and discussion section is separated into four parts. Based on our previous study, first, we provide further complementary information on the structural properties of Au oxide structures obtained by HV electrolysis as well as the NPG films obtained by subsequent electrochemical reduction. Second, we discuss the impact of H₂O₂ concentration (in 0.01 M KOH) and temperature on the reduction of Au oxide films formed by HV electrolysis at 300 V. Third, we show the impact of the electrolysis voltage and the electrolyte temperature on the change in surface area of the NPG films after electrochemical reduction. Finally, we discuss the impact of

the electrolysis time on the change in electrolyte temperature and, more importantly, on the structure formation.

Structural Properties

The structural properties of Au electrodes after HV electrolysis were investigated on wire and sheet Au anodes. The choice of the electrode type depends on the analytical approaches employed (see experimental section). In this section, we studied Au sheet electrodes modified by HV electrolysis at 300 V for 290 s, which were (i) directly removed from the electrolysis solution or (ii) subsequently reduced electrochemically, as reported previously.^[36] At 300 V the structural changes are most significant, compared to lower voltages or voltages in the aCGDE region. Nevertheless, the following observations are also representative for other voltages in the range of 100 to 540 V.

Upon direct removal of the Au electrode from the electrolysis solution, the electrode's color is red, while the reduced electrode is black as illustrated in the optical microscope images in Figures 1a and b. Previously, we suggested that the red color is related to the formation of a Au₂O₃ film. This assumption is confirmed by XPS measurements of the Au 4f region shown in Figure 1c. The spectrum clearly shows features related to Au⁰ (binding energies – BE: 84.0 eV and 87.7 eV^[42–45]) and Au³⁺ (BE: 85.8 eV and 89.5 eV^[42,43]), where the latter is significantly more pronounced. A contribution from Au⁺, which should appear between the features of Au⁰ and Au³⁺, is not measurable. Au⁺ would possibly be related to Au₂O, which is considered to be a metastable intermediate during the reduction of Au₂O₃.^[46,47] The Au⁰ feature in the Au 4f region can be attributed to areas that are not covered with Au oxide, resulting from the detachment of the Au oxide film from the Au substrate during the transfer (compare Figure 1a lower right edge). Plausibly, the Au oxide also decomposes during the XPS measurement due to beam damage.^[48] In the O 1s region (see Figure S1), a typical oxidic oxygen state is observed as the main feature, which is most likely related to Au₂O₃.^[49,50] The peak is, however, relatively broad compared to pure metal oxides, which, in general, is indicative for defects in the oxide. A second feature visible in the O 1s region can be ascribed to OH species.

The black color of the reduced electrodes was suggested to originate from a nanoporous Au (NPG) structure.^[21,31–33,51] A corresponding XPS spectrum of the Au 4f region is shown in Figure 1d. The spectrum clearly shows that the electrode consists primarily of metallic Au⁰. Minor contributions from oxidic Au⁺- and Au³⁺-species are also present. The corresponding O 1s peak has a much lower intensity than that of the oxidic sample. Nevertheless, the peak still consists of two features, which were ascribed to oxidic oxygen and OH (as discussed above and described along with Figure S1).

Corresponding SEM images of both electrodes are shown in Figures 1e and f. The image taken on the red electrode shows a relatively flat surface with some large cracks, while the images of the black electrode (after electrochemical

reduction) exhibit, in addition to the large cracks, a more patterned structure. Further SEM images of Au electrodes formed by HV electrolysis at 300 V are provided in Figure S2. Cross-sectional SEM images of both the red and black electrodes in Figures 1g and h, provide further information on the film thickness and structure. The schematic illustration shows the different regions of the cross-section, where the part above the dashed line shows the surface. The cross-section of the Au_2O_3 film (Figure 1g) shows a several 100 nm thick porous film. Note, however, that cutting the sample with an ion beam could also damage the structures and lead to the formation of porous structures observed in the Au oxide. The NPG film obtained by electrochemical reduction depicted in Figure 1h shows a more ordered porous structure with mostly vertically aligned pores. To be able to estimate the pore and ligament size of the NPG structures formed in this work more precisely, SEM images of the NPG structures with high resolution and magnification after 30 s at 300 V, as well as 540 V are shown in Section S3.

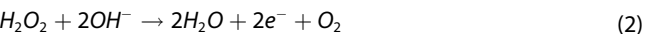
H_2O_2 Concentration and Temperature Dependence

As described above, the Au oxide formed during HV electrolysis is reduced when the electrode is kept in the electrolysis solution after HV electrolysis. It was suggested that the reduction process is caused by H_2O_2 in the electrolyte^[36,40], which forms during HV electrolysis.^[38,39,41] The general ability of H_2O_2 to reduce Au cations is already known in literature and can be explained by using the standard electrochemical potentials.^[25–27,29] Therefore, we suggest the following reactions.

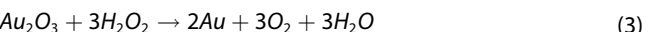
Reduction:



Oxidation:



Overall reaction:



To illustrate the role of H_2O_2 in the reduction of the Au oxide, we investigated changes in the surface structure induced by i) H_2O_2 -containing KOH solutions of different concentration at constant temperature and ii) by varying the H_2O_2 solution temperature for a constant H_2O_2 concentration. In the following a “ H_2O_2 solution” refers to a “ H_2O_2 -containing 0.01 M KOH solution”. All H_2O_2 concentrations are referred to weight %. Table S4 summarizes the following experimental conditions, observations, and evaluated RFs.

For these investigations, the Au oxide films were prepared on Au wire electrodes in 0.01 M KOH at 300 V for 30 s. The electrodes were directly removed from the electrolysis solution to minimize the reducing effect from the H_2O_2 in the electrolysis solution.

The concentration dependence was studied by immersing the Au oxide-covered electrodes at room temperature for 60 s in H_2O_2 -containing KOH solutions with concentrations of 0.007 %, 0.08 %, and 0.8 %. Upon removal from a 0.007 % H_2O_2 -containing 0.01 M KOH solution, the electrode still appears red, whereas, in a 0.08 % and 0.8 % H_2O_2 -containing 0.01 M KOH solution, the electrodes turn black within 60 s.

Corresponding SEM images of the electrodes are shown in Figure 2 with large-scale images in the top row and regions with higher magnification of these surfaces in the bottom row.

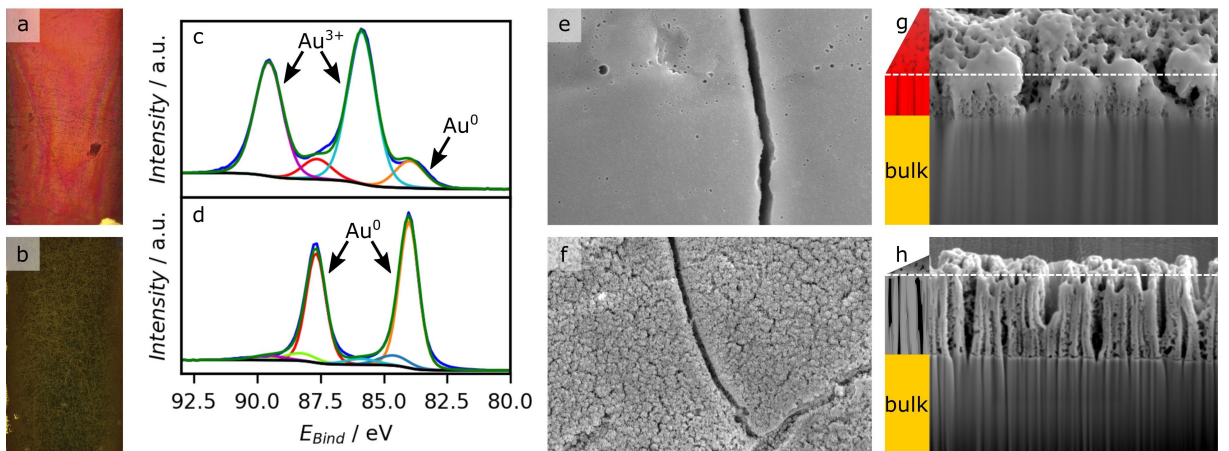


Figure 1. Top row: Structural properties of a Au sheet electrode after electrolysis at 300 V for 290 s in 0.01 M KOH. Bottom row: A Au sheet electrode which was reduced electrochemically after HV electrolysis. a) and b) show corresponding optical microscope images. c) and d) show XPS spectra of the Au 4f region, including the peaks fitted to Au^0 and Au^{3+} . e) and f) show top-view SEM images with image sizes of 6 $\mu\text{m} \times 4 \mu\text{m}$. g) and h) show cross sectional SEM images of the surfaces in e) and f) with image sizes of 4 $\mu\text{m} \times 3 \mu\text{m}$ and 8 $\mu\text{m} \times 6 \mu\text{m}$. The schematic illustration next to the cross sectional SEM images show the color of the sheets and the viewing angle during the image acquisition.

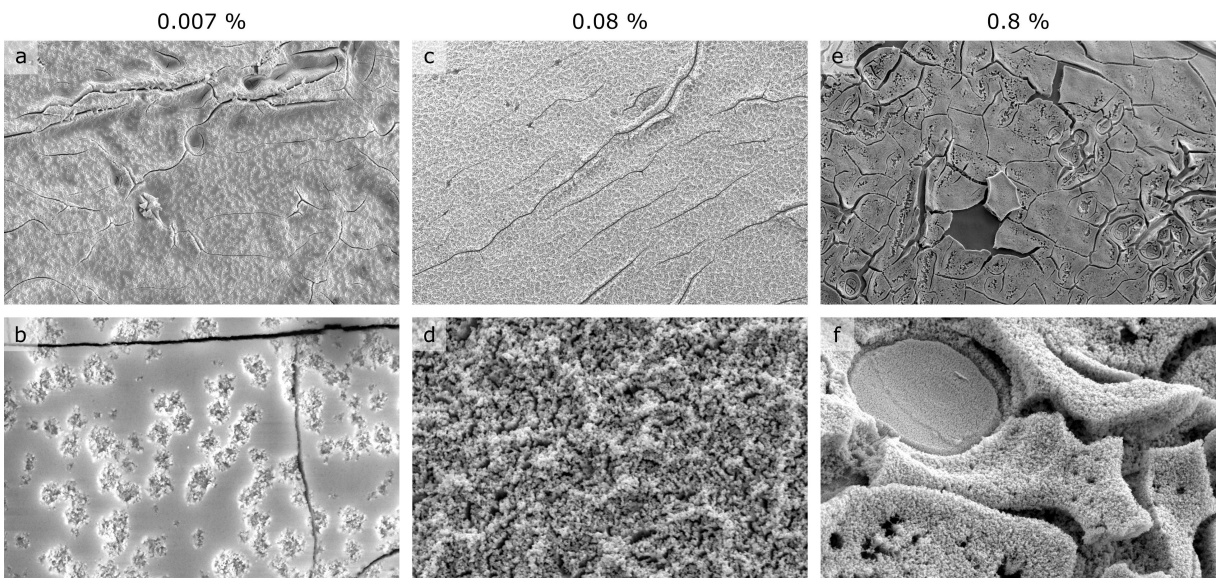


Figure 2. SEM images recorded on Au wire electrodes after electrolysis at 300 V for 30 s, direct removal from the electrolysis solution and subsequent reduction for 60 s in H_2O_2 -containing 0.01 M KOH solutions (room temperature). The amount of H_2O_2 is given above the respective columns. The top row images show sizes of $120 \mu\text{m} \times 80 \mu\text{m}$ and the bottom row $12 \mu\text{m} \times 8 \mu\text{m}$.

It is apparent that the structure formation strongly depends on the H_2O_2 concentration. The electrode surface upon removal from the 0.007% H_2O_2 solution (Figures 2a and b) still appears rather smooth and is only restructured in certain regions. Interestingly, it seems that the restructuring process starts in random regions on the surface, which are separated by about $0.5 \mu\text{m}$. For electrodes immersed in a 0.08% H_2O_2 solution (Figures 2c and d), the entire surface is nanostructured. Increasing the concentration further by one order of magnitude (0.8% H_2O_2 – Figures 2e and f), large cracks appear on the surface. In some regions, the surface even peels off (Figure 2e), in others, large protrusions form on the surface (Figure 2f). The amount of oxide remaining on the electrode after removal from a H_2O_2 solution was determined by electrochemical reduction of the electrodes. The electrodes removed from low-concentrated H_2O_2 solutions still show a current density related to oxide reduction. This current density is significantly lower compared to that recorded on electrodes reduced electrochemically directly after the HV electrolysis. The electrode immersed in 0.8% H_2O_2 solution is completely reduced after 60 s.

Even though H_2O_2 seems to play a critical role in the reduction of the Au oxide, the structures obtained after HV electrolysis and subsequent electrochemical reduction (compare with Figure 1f) do not resemble those observed upon immersion of the Au oxide in H_2O_2 solutions. Possible reasons for this discrepancy are that after HV electrolysis, the H_2O_2 concentration will be high in the region around the electrode and will decrease with increasing time, as shown elsewhere.^[40] Furthermore, during HV electrolysis, the temperature of the electrolyte will increase,^[39,41,52,53] which could also be a decisive factor for the structure formation.

To separate the effect of temperature and H_2O_2 concentration on the structure formation, Au oxide electrodes prepared by HV electrolysis at 300 V were immersed for 60 s in a freshly prepared 0.01 M KOH solution heated to 70 °C. Afterward, the electrode's color was still red, indicating that the Au oxide is stable at this temperature in pure 0.01 M KOH. This result is in line with the findings by Tsai et al. who studied the kinetics of dissociation of Au_2O_3 at different temperatures.^[54] Hence, we can exclude that temperature alone has an effect on the transformation of Au oxide to pure Au or other structural changes of the electrode.

To study the influence of the combined effect of temperature and H_2O_2 on the NPG structure formation, Au oxide electrodes were immersed for 60 s in 0.007% H_2O_2 solutions with electrolyte temperatures of 24, 40, and 70 °C. Au oxide electrodes immersed in a 0.007% H_2O_2 solution at 24 °C or 40 °C remained red. At 70 °C, the color of the electrodes turned black with a touch of red. In all three cases, additional electrochemical reduction of the electrodes revealed that the electrodes still contained a significant amount of Au oxide. Hence, under these conditions, the electrodes do not reduce completely.

Corresponding SEM images of the resulting electrode surfaces are shown in Figure 3 with large-scale images in the top row and magnified regions of these surfaces in the bottom row. The conditions in Figures 3a and b are identical to those in Figures 2a and b and are only shown for comparison. The main observation is that the restructuring becomes more pronounced with higher temperature and that the number of cracks, observed already at room temperature, increases. Despite the significant restructuring, the surface structure is not identical to that obtained by HV electrolysis at 300 V and

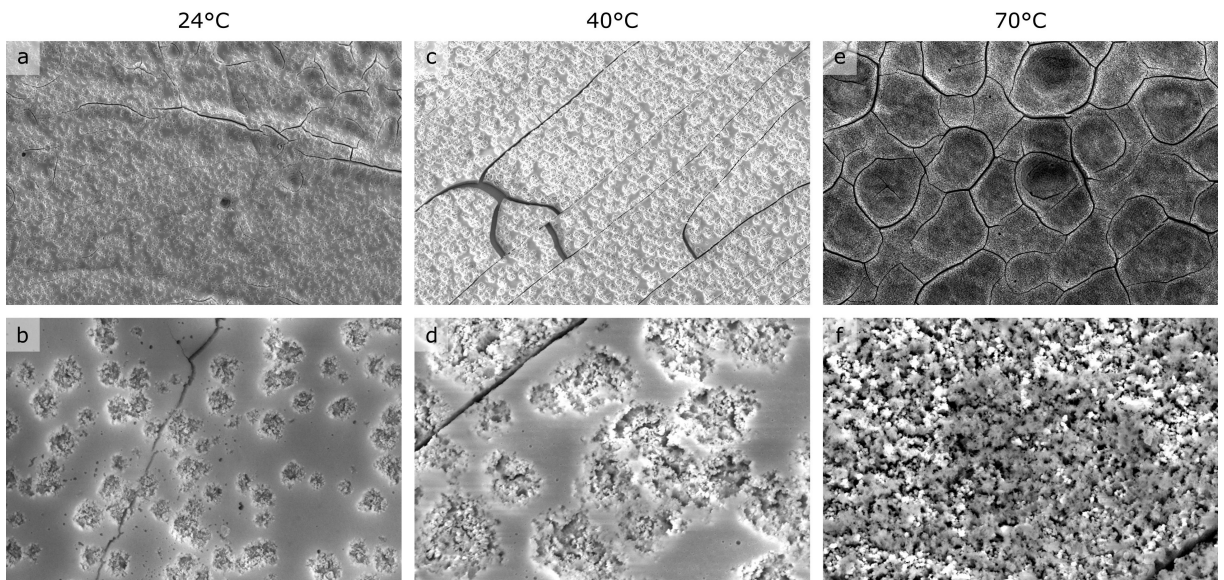


Figure 3. SEM images of Au wires after HV electrolysis at 300 V for 30 s and direct removal from the electrolysis solution with subsequent reduction through immersion in 0.01 M KOH solutions with a H_2O_2 concentration of 0.007% for 60 s and temperatures of a) and b) 24 °C (room temperature), c) and d) 40 °C and e) and f) 70 °C. The image size of a), c) and e) is 120 $\mu\text{m} \times 8 \mu\text{m}$, from b), d) and f) 12 $\mu\text{m} \times 8 \mu\text{m}$.

subsequent electrochemical reduction (see Figures 5a to d) or reduction in the electrolyte.

Overall, these results show that the H_2O_2 concentration and temperature play a major role in structure formation. This is an important aspect since these parameters change dynamically and in an uncontrolled way when the electrodes are kept in the electrolysis solution after HV electrolysis, i.e., the H_2O_2 concentration will probably decrease due to dissipation in the electrolyte,^[40] and the local temperature will also decrease due to heat dissipation into the surrounding electrolyte.

Effect of HV Electrolysis Parameters – Voltage and Temperature

In the following, we demonstrate and discuss how the surface area of the NPG film can be controlled by tuning the electrolysis voltage and electrolyte temperature. In our previous work, we demonstrated that independent of the applied voltage during HV electrolysis, the resulting Au oxide surface structures appear rather similar, as well as the fully-reduced Au oxide structures (also shown in an additional set of SEM images in Figure S5). The change in surface area, here discussed based on the roughness factor (RF – see Experimental Section), of the NPG film, however, depends on the electrolysis voltage and correlates with the average current density during HV electrolysis.^[36] A corresponding $j-U$ curve (dark blue solid line) is shown along with the RF (dark blue dashed line) in Figure 4. Note that each point in the plot represents an individual measurement on a freshly-prepared Au wire, where the voltage was applied for 30 s, and the

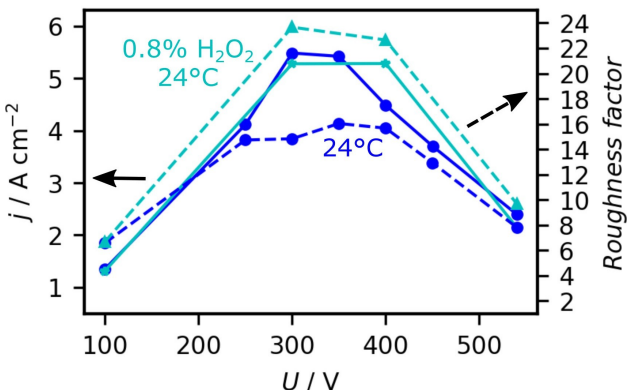


Figure 4. HV electrolysis of a Au wire electrode for 30 s at different voltages and an initial electrolyte temperature of 24 °C in 0.01 M KOH and subsequent electrochemical reduction (dark blue), as well as reduction by immersion of the electrode for 60 s in a 0.8% H_2O_2 -containing 0.01 M KOH solution at 24 °C (cyan). The average current densities during HV electrolysis are shown by the points linked by solid lines, the roughness factors of the electrode after HV electrolysis and following reduction are shown by the points linked by dashed lines.

electrode was subsequently reduced electrochemically. Overall, the $j-U$ characteristic is described in the literature.^[4,39,52,55–57] Thus, only the most important aspects are briefly introduced here.

For gas-evolving electrodes, the $j-U$ curve can be divided into different regions. First, the current increases linearly with increasing voltage (Ohmic behavior) up to a certain breakdown voltage (V_B). Here, bubble formation becomes significant, and a gas sheath starts to form around the electrode, which increases the resistance at the electrode | electrolyte

interface and hence leads to a decrease in current density. With increasing voltage, the gas film becomes more stable, showing partial ionization of the gas in the sheath (partial aCGDE). At the midpoint voltage (V_D , here ca. 540 V), full aCGDE is observed.

First, to demonstrate possible differences between the electrochemical reduction and reduction by H_2O_2 on the RF, Au oxide samples were prepared at different voltages as described above and were reduced in an 0.8% H_2O_2 solution. At this H_2O_2 concentration, the reduction process was suggested to be complete. The corresponding $j-U$ curve (cyan solid line) resulting from the electrolysis of the Au electrodes is shown in Figure 4, which shows a similar behavior to the

curve in dark blue (illustrating the reproducibility of the approach). The RF of the Au oxide films reduced in the H_2O_2 solution is shown by the cyan dashed curve in Figure 4.

Comparing the RF of the Au oxide reduced electrochemically with that reduced in a H_2O_2 solution (dashed blue and cyan curves in Figure 4), the values are rather similar for Au electrodes treated by low and high electrolysis voltages. For intermediate electrolysis voltages around V_B , the Au oxides reduced in H_2O_2 have a larger RF than the electrochemically reduced Au oxides. This is also apparent from SEM images, where the NPG film formed by reducing Au oxide in a 0.8% H_2O_2 solution shown in Figures 5e–h is much more inhomogeneous than the electrochemically reduced film in Figures 5a–d.

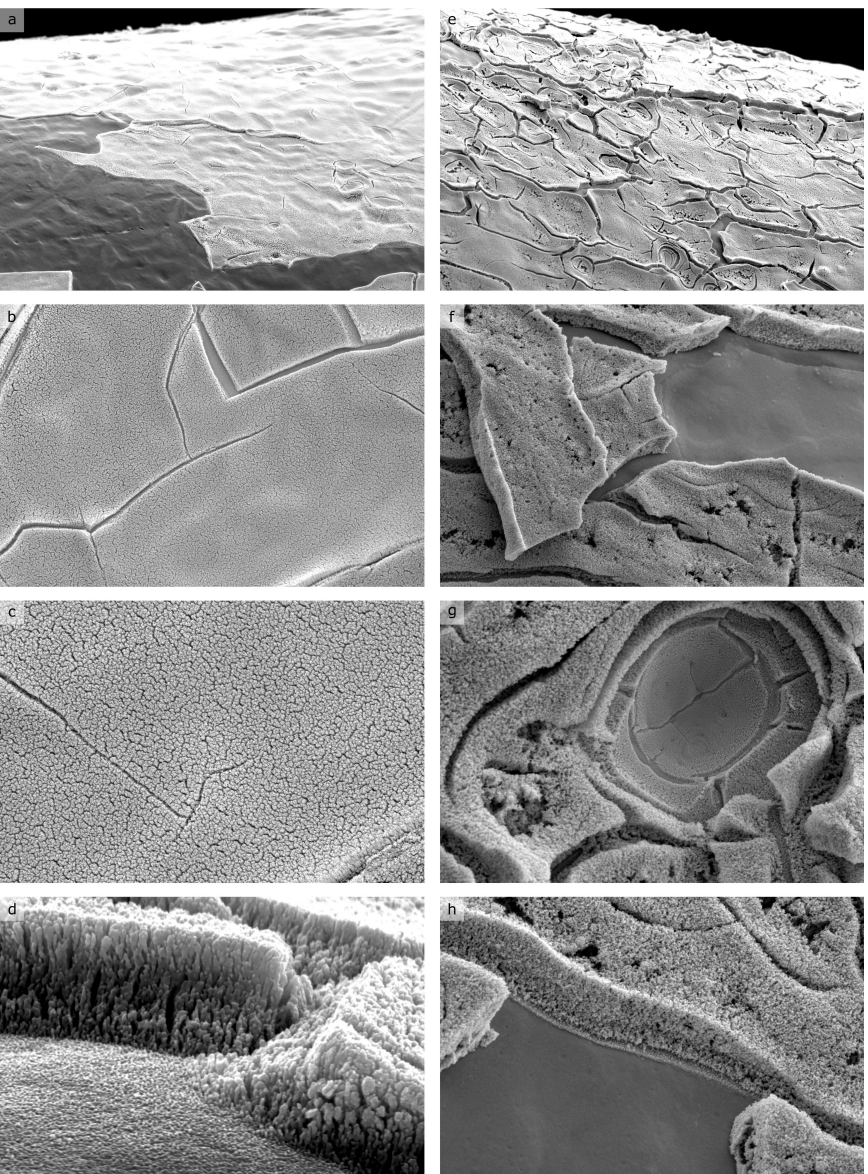


Figure 5. SEM images of Au wire electrodes after HV electrolysis at 300 V for 30 s and a) to d) subsequent electrochemical reduction, or e) to h) reduction in a 0.8% H_2O_2 -containing 0.01 M KOH solution. The image size in a) and e) is 120 $\mu\text{m} \times 80 \mu\text{m}$, b) and f) 30 $\mu\text{m} \times 20 \mu\text{m}$, c) and g) 12 $\mu\text{m} \times 8 \mu\text{m}$ and d) 3 $\mu\text{m} \times 2 \mu\text{m}$.

The effect of the electrolysis solution temperature on the RF of NPG films after the electrochemical reduction of Au oxide films is illustrated in Figure 6 by the dashed lines (24°C – blue, 46°C – orange and 70°C – red). The corresponding j – U curves are shown by the solid lines. At higher initial electrolyte temperatures, the breakdown voltage (V_B) shifts to lower voltages. This shift can be explained by the fact that the boiling point of the electrolyte is reached on a shorter timescale at a higher initial electrolyte temperature.^[39,53,58,59] In addition, the average current densities at low voltages increase due to an increase in ion conductivity in the electrolyte, whereas at high voltages, the current densities decrease with the temperature due to more facile gas sheath formation. More detailed information on the effect of the initial electrolyte temperature on the j – U curves can be found elsewhere.^[39,53,58–60] Further information on the increase in electrolyte temperature at different initial electrolyte temperatures during HV electrolysis is explained along with Figure S6.

More importantly, after the electrochemical reduction, the evolution of the RF with applied voltage follows the evolution of the average current density for all temperatures and applied voltages. The largest increase in surface area is observed for low initial electrolyte temperatures and voltages in the range of V_B . For low and high voltages, the differences in RF at different initial electrolyte temperatures are less significant. In addition, for high voltages in the aCGDE region (≥ 450 V), the RF does not increase significantly compared to bare Au electrodes at higher initial electrolyte temperatures. Therefore, NPG films with high surface area are achieved for low initial electrolyte temperatures.

Time Dependence

To illustrate the impact of electrolysis time on the Au oxide formation and the RF of the final NPG film, we performed

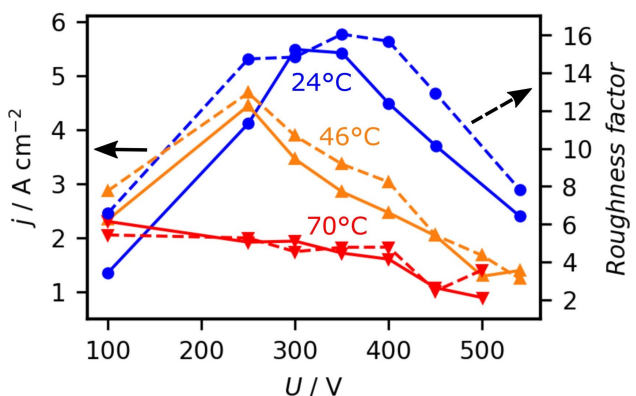


Figure 6. HV electrolysis of a Au wire electrode for 30 s at different voltages and initial electrolyte temperatures (24°C – blue, 46°C – orange and 70°C – red) in 0.01 M KOH. The j – U traces are connected with solid lines, while the corresponding RF after electrochemical reduction are connected with dashed lines. Each data point marks an individual measurement. The current densities are averaged over 30 s (see experimental section). The lines only serve as a guide to the eye.

electrolysis experiments at 300 V and 540 V for different times ranging from 10 to 600 s. The 300 V experiments were also performed at 46°C and 70°C . Since the 300 V measurements could not be performed without complications (see below), we first discuss the results obtained for 540 V.

Figure 7a shows the evolution of the current density during 600 s HV electrolysis at 540 V (black line). The curves for shorter electrolysis times are not shown but they look very similar and follow the same trend. At the start of the measurement, the current density rises sharply, reaching a maximum within a second (see inset in Figure 7a). Immediately, strong bubble formation is observed, followed by the formation of a dynamic gas layer around the electrode. Furthermore, at this voltage a plasma develops in the resulting gas layer between the electrode surface and the electrolyte. With increasing time, the current drops until it becomes almost constant for longer electrolysis times (ca. 100 s).

The evolution of the structural properties was determined from several experiments with different electrolysis times on freshly prepared electrodes. For each sample, Figures 7b and c show (i) the amount of Au oxide formed during HV electrolysis

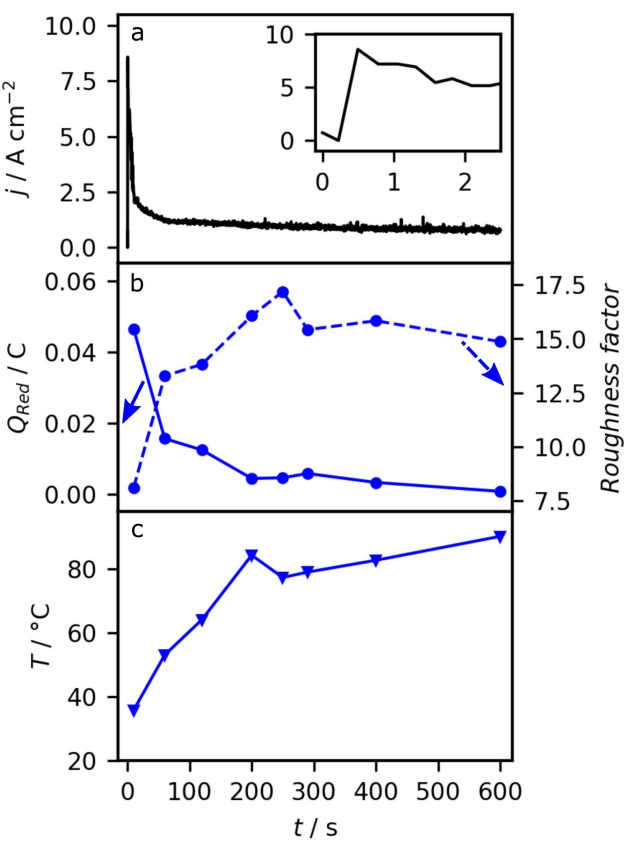


Figure 7. Time dependence of HV electrolysis on a Au wire electrode at 540 V in 0.01 M KOH. a) Current density during HV electrolysis. b) Amount of Au_2O_3 formed after different HV electrolysis times determined by electrochemical reduction (solid line) and RF (dashed line) of the NPG film. c) Electrolyte temperature after HV electrolysis (initial electrolyte temperature: 24°C).

(Figure 7b – solid), (ii) the RF of the electrodes after electrochemical reduction (Figure 7b – dashed), and (iii) the electrolyte temperature after electrolysis (Figure 7c). The starting electrolyte temperature was, in each case, room temperature. For short electrolysis times (10 s) the amount of Au oxide is high (Figure 7b – solid), which decreases with longer electrolysis times exponentially. From approximately 200 s onward, the amount of Au oxide on the surface is very low and almost negligible at 600 s. In turn, the RF follows an opposite trend, whereby in the first 30 to 60 s, the RF of the NPG electrodes increases sharply. For longer electrolysis times, the increase in RF becomes smaller, reaching a plateau after approximately 200 s where the surface area is 15 times larger compared to that of the bare Au electrode. With increasing electrolysis time, the temperature rises up to ca. 80 °C within 200 s and increases only slightly within the next 400 s. By comparing all measurements in Figure 7, it is apparent that the amount of Au_2O_3 is not directly correlated with the increase in surface area obtained after the electrochemical reduction. Thus it seems that the Au oxide is reduced automatically, as discussed further below. More importantly, this set of measurements suggests, that the formation of NPG films via HV electrolysis does not necessarily require an additional step to reduce a Au oxide, but it can be formed directly via HV electrolysis when the electrolysis time is sufficiently long.

While a full explanation for the observed behavior is still missing, the following aspects can be excluded or considered to be at the origin. First, we often observed (also in previous measurements) that parts of the newly formed films (Au oxide or NPG) peeled off from the substrate surface during HV electrolysis. If this effect would be significant, especially at long electrolysis times, we would not only expect that the amount of Au oxide on the surfaces decreases but also the roughness factor will decrease (or both should be correlated with one another). Hence this aspect can be ruled out. Second, with increasing electrolysis time, the amount of H_2O_2 in the solution will increase, which in turn would increase the probability of reducing the Au oxide. However, performing electrolysis at 540 V leads to the formation of a gas sheath around the electrode, and hence the contact area between the electrode and electrolyte can be considered to be negligible. Whether or not H_2 , which also forms under these conditions and might be present in the sheath,^[41,58,61] plays a role is questionable. Based on separate experiments, where we immersed a Au oxide electrode in a H_2 -containing 0.01 M KOH solution, we did not observe a reduction of the Au oxide. Third, during the electrolysis, not only does the electrolyte temperature increase, but most likely also that of the electrode. Under certain circumstances, the electrodes might even melt during aCGDE conditions.^[39,53] Considering that the decomposition temperature of Au_2O_3 is only approximately 150 °C,^[46,49,54] it is likely that the Au oxide decomposes to Au due to the high local electrode temperature. Overall, we suggest that this is presumably the most likely scenario.

We performed a similar set of experiments at an electrolysis voltage of 300 V and in electrolytes initially at room temperature. In contrast to electrolysis at 540 V, the

averaged current densities during HV electrolysis are much higher, and the electrode is still, to some extent, in contact with the electrolyte, despite vivid bubble formation. The amount of H_2O_2 formed at this voltage may also differ from that formed at 540 V, since the literature only reports H_2O_2 formation above the midpoint voltage. However, we were recently able to show that H_2O_2 is most likely also formed at lower voltages and at 300 V.^[36] The temporal evolution of the current density recorded at 300 V is shown in red in Figure 8 together with that recorded at 540 V in black. The inset shows the increase in current density at the beginning of the HV electrolysis.

A key issue in the experiments performed at 300 V was that for longer electrolysis times, the films formed on the surface significantly peeled off. Therefore, we limit ourselves to a more qualitative description. After 120 s of HV electrolysis, the electrode exhibits a red color, indicating that the electrode is covered with a Au oxide film. After the electrochemical reduction, the RF of the NPG electrode is larger compared to the bare Au electrode. From visual inspection, it is apparent that for longer electrolysis times (290 s up to 600 s), the Au oxide or NPG film significantly peeled off from the electrode and the electrode appears mostly golden. The RF determined after the electrochemical reduction is very low compared to the electrode which was treated by electrolysis for only 120 s. But since the resulting film seemed to peel off, this result is not very meaningful, except that it underlines that no Au oxide or NPG can be formed under these conditions, i.e. at long electrolysis times. To what extent the rise of the electrolyte temperature up to 80 °C or the vivid bubble formation plays a role in the removal of the films is unclear. Hence, at high current densities and during HV electrolysis with bubble formation, short time scales are required to form a stable Au oxide film, which can then be reduced in a second step to form a NPG film.

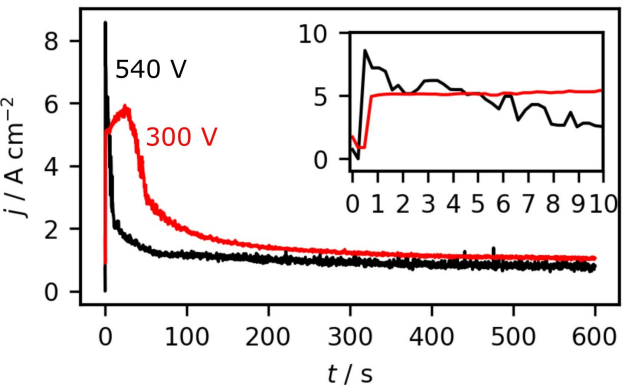


Figure 8. Evolution of the current density with time during HV electrolysis at 540 V (black) and 300 V (red) in 0.01 M KOH.

Conclusion

In this work, we demonstrated that NPG can be prepared by a simple and fast method, namely by (i) HV electrolysis alone or followed by (ii) electrochemical reduction or (iii) reduction in an H_2O_2 -containing KOH solution. The thickness of the NPG film and surface structure can be controlled by several parameters:

1. The voltage applied during HV electrolysis.

2. The initial electrolyte temperature before HV electrolysis. The lower the initial electrolyte temperature, the greater is the surface area of the resulting NPG film, when the current densities during HV electrolysis are higher at low initial electrolyte temperatures.

3. The electrolysis time in the region of aCGDE. With short electrolysis times, the surface area increases sharply within a very short time period (30 to 60 s), while for longer electrolysis times the surface area remains almost constant.

Reduction of the Au_2O_3 films previously formed by HV electrolysis on the electrode surfaces in H_2O_2 solutions of different concentrations and temperatures additionally leads to different surface areas and surface structures. Depending on the application, these differences in surface structure and surface area should be considered during the preparation of NPG films in order to assess its impact for possible applications. HV electrolysis thus represents a suitable "green chemistry"-approach to produce well adaptable NPG films in a fast and efficient way.

Experimental

Materials

All Au wires used have a diameter of 0.5 mm (MaTeck, 99.99%). The Au sheets have a thickness of 0.127 mm (MaTeck, 99.99%).

The 0.01 M KOH solution used as an electrolyte was prepared from KOH pellets (Sigma-Aldrich, 99.99%) and Milli-Q water ($18.2\text{ M}\Omega\text{ cm}$, TOC $\leq 3\text{ ppb}$). The 1 M HCl solution used for electro-polishing was prepared from a 30% HCl (Suprapur, Merck). The H_2O_2 solutions were prepared from a 50 wt.% H_2O_2 solution (Acros Organics) stabilised in water. For all H_2O_2 containing solutions, the concentrations are referred to wt.%.

Sample Preparation

For each measurement, the Au wire/sheet was heated in a propane flame (MTI) for 3 min to remove impurities and flatten the surface. Wire electrodes with a highly restructured surface after the experiment were additionally electropolished in 1 M HCl at 10 V vs. a graphite electrode and subsequently annealed for 3 min. In the case of the Au sheets, a new piece was used for each measurement to ensure similar starting conditions.

Electrolysis Cell

The HV electrolysis experiments were performed in a glass cell filled with 60 mL of 0.01 M KOH. For XPS and cross-sectional SEM imaging Au sheets were used instead of Au wires in order to have

larger surfaces and circumvent issues with the curvature of the electrodes posing problems for further analytics. The Au wire or sheet used as plasma working electrode (PWE) was placed 2.5 cm apart from the plasma counter electrode (PCE), made from a stainless steel plate (15 mm \times 20 mm \times 3.5 mm). Usually, 10 mm of the wire were immersed in the electrolyte (surface area: 0.16 cm^2). Depending on the measurement, a sheet (2 mm \times 12.5 mm) was immersed either 4 mm (surface area: 0.1727 cm^2) or 10 mm in the electrolyte (surface area: 0.4280 cm^2). The voltage was applied with a TDK-Lambda Power Supply (630 V/1.365 A) which was controlled with a LabVIEW software. The temperature of the electrolyte was measured before and after the electrolysis. In addition, the electrolyte was exchanged after each measurement to avoid possible changes of the initial conditions (electrolyte temperature, dissolved products, etc.). Moreover, all HV electrolysis experiments were performed without stirring the electrolyte.

The current densities shown in Figures 4 and 6 are averages over the entire electrolysis time.

Electrochemical Cell

The electrochemical measurements were performed in a glass beaker^[36] containing 150 mL of 0.01 M KOH. Before starting the measurements, the electrolyte was deaerated with N_2 . All electrochemical measurements were performed without stirring the electrolyte. A homemade reversible hydrogen electrode (RHE) served as reference electrode, the Au wire and sheets used for the electrolysis experiments were used as working electrodes and a Pt-sheet (10 \times 7.5 mm) as electrochemical counter electrode. The measurements were controlled with an FHI ELAB potentiostat.

Experimental Procedure

Two separate cells were used for the HV electrolysis and the electrochemical characterization since during HV electrolysis, the electrolyte properties change (O_2 accumulation, increase in H_2O_2 content, change in temperature), which does not allow recording reliable electrochemical results.

The current densities of the electrochemical measurements were obtained by relating the currents during the measurements to the original geometric surfaces of the samples. For each electrochemical measurement, the initial potential was set to 1.1 V. With a scan rate of 50 mV s^{-1} , the potential was subsequently decreased (negative scan direction). The potential was then cycled between 0.20 V and 1.69 V.

To reduce the Au oxide produced by HV electrolysis electrochemically, the potential was also decreased gradually with a scan rate of 50 mV s^{-1} starting from an initial potential of 1.1 V. At a potential of 0.25 V, it was then held in the first negative scan until the additional current present due to the reduction of the Au oxide had disappeared. Integrating this reductive current provides the charge related to the reduction of Au oxide. A detailed description of the experimental procedure can also be found in Ref. [36].

For the preparation of the samples for cross-sectional SEM imaging, the complete reduction was performed by holding the potential immediately at 0.25 V.

To determine the change of electrochemical surface area (ECSA) of the NPG films, we performed CV measurements before and after HV electrolysis. This will also reduce the remaining Au oxide from the surface. The change in surface area was determined in each case from the thickness of the double layer at 0.87 V. At this

potential, neither Faraday reactions nor adsorption processes take place. Exemplary CVs recorded before and after the electrolysis/reduction experiment are shown in Figure S7. The ratio between the values of the double layer before and after is denoted as roughness factor (RF), which in other words, describes the relative change in surface area compared to a bare Au electrode.

Structural Characterization

All SEM images were recorded with a Quattro S scanning electron microscope (SEM) from Thermo Scientific. An accelerating voltage of 10 kV or 20 kV was used to record the images. The cross-sectional SEM images were taken with a Scios2 from Thermo Scientific. A Ga source was used for surface milling to get the cross sections. The SEM images taken from the cross sections were recorded at an acceleration voltage of 10.00 kV. The microscope images of the Au electrodes were taken with a Leica S9i microscope, also from Thermo Scientific.

XPS

All XPS measurements were performed using monochromatic Al K_α (1486.6 eV) radiation. The signals were detected at an angle of 45°. To avoid possible charging effects, all XPS samples were measured with a neutralizer as a precaution, although all samples had metallic contact with the ground.

Credit

E. Artmann: Conceptualization, Formal Analysis, Funding Acquisition, Investigation, Validation, Visualization, Writing – Original Draft Preparation. L. Forschner: Investigation, Writing – Review & Editing. K. M. Schüttler: Investigation, Writing – Review & Editing. Dr. M. Al-Shakran: Investigation. Prof. Dr. T. Jacob: Funding Acquisition, Resources, Supervision, Writing – Review & Editing. Dr. A. K. Engstfeld: Funding Acquisition, Conceptualization, Supervision, Writing – Review & Editing

Acknowledgment

This work was funded by the SFB-CRC1316 of the DFG (German Research Foundation). Further, support by the state of Baden-Württemberg and the DFG through grant no INST 40/574-1 FUGG is gratefully acknowledged. E. A. would like to thank the “Stiftung Stipendien-Fonds des Verbandes der Chemischen Industrie (VCI)” for the financial support in the form of a scholarship. The authors also want to thank Joachim Bansmann for his support with the XPS measurements. Open Access funding enabled and organized by Projekt DEAL.

Conflict of Interest

The authors declare no conflict of interest.

Data Availability Statement

The data that support the findings of this study are openly available in Zenodo at <http://doi.org/10.5281/zenodo.6973687>.

Keywords: Contact Glow Discharge Electrolysis · Electrolysis · Gold · Gold oxide · Nanoporous Gold

- [1] T. Juarez, J. Biener, J. Weissmüller, A. M. Hodge, *Adv. Eng. Mater.* **2017**, 19, 1700389.
- [2] J. Zhang, C. M. Li, *Chem. Soc. Rev.* **2012**, 41, 7016.
- [3] I. McCue, J. Stuckner, M. Murayama, M. J. Demkowicz, *Sci. Rep.* **2018**, 8, 6761.
- [4] R. Akolkar, R. M. Sankaran, *J. Vac. Sci. Technol. A* **2013**, 31, 050811.
- [5] K. Yan, P. Karthick Kannan, D. Doonyapisut, K. Wu, C.-H. Chung, J. Zhang, *Adv. Funct. Mater.* **2021**, 31, 2008227.
- [6] D. Jalas, L.-H. Shao, R. Canchi, T. Okuma, S. Lang, A. Petrov, J. Weissmüller, M. Eich, *Sci. Rep.* **2017**, 7, 44139.
- [7] J. K. Bhattachari, D. Neupane, B. Nepal, V. Mikhaylov, A. V. Demchenko, K. J. Stine, *Nanomaterials* **2018**, 8.
- [8] S. H. Kim, *Curr. Appl. Phys.* **2018**, 18, 810.
- [9] S. Xiao, S. Wang, X. Wang, P. Xu, *Nano Select* **2021**, 2, 1437.
- [10] J. Biener, A. Wittstock, L. A. Zepeda-Ruiz, M. M. Biener, V. Zielasek, D. Kramer, R. N. Viswanath, J. Weissmüller, M. Bäumer, A. V. Hamza, *Nat. Mater.* **2009**, 8, 47.
- [11] J. Biener, M. M. Biener, R. J. Madix, C. M. Friend, *ACS Catal.* **2015**, 5, 6263.
- [12] A. Wittstock, A. Wichmann, J. Biener, M. Bäumer, *Faraday Discuss.* **2011**, 152, 87.
- [13] X. Zhang, Y. Ding, *Catal. Sci. Technol.* **2013**, 3, 2862.
- [14] Z. Wang, S. Ning, P. Liu, Y. Ding, A. Hirata, T. Fujita, M. Chen, *Adv. Mater.* **2017**, 29.
- [15] P. Liu, P. Guan, A. Hirata, L. Zhang, L. Chen, Y. Wen, Y. Ding, T. Fujita, J. Erlebacher, M. Chen, *Adv. Mater.* **2016**, 28, 1753.
- [16] T. Fujita, P. Guan, K. McKenna, X. Lang, A. Hirata, L. Zhang, T. Tokunaga, S. Arai, Y. Yamamoto, N. Tanaka, Y. Ishikawa, N. Asao, Y. Yamamoto, J. Erlebacher, M. Chen, *Nat. Mater.* **2012**, 11, 775.
- [17] D. Li, Y. Zhu, H. Wang, Y. Ding, *Sci. Rep.* **2013**, 3, 3015.
- [18] A. Goyal, C. J. Bondué, M. Graf, M. T. M. Koper, *Chem. Sci.* **2022**, 13, 3288.
- [19] C. Zhu, Z. Qi, V. A. Beck, M. Luneau, J. Lattimer, W. Chen, M. A. Worsley, J. Ye, E. B. Duoss, C. M. Spadaccini, C. M. Friend, J. Biener, *Sci. Adv.* **2018**, 4, eaas9459.
- [20] Y. Ding, M. Chen, *MRS Bull.* **2009**, 34, 569.
- [21] R. Zhang, H. Olin, *Materials* **2014**, 7, 3834.
- [22] E. Seker, J. T. Gaskins, H. Bart-Smith, J. Zhu, M. L. Reed, G. Zangari, R. Kelly, M. R. Begley, *Acta Mater.* **2007**, 55, 4593.
- [23] E. Seker, M. Reed, M. Begley, *Mater.* **2009**, 2, 2188.
- [24] K. Nishio, H. Masuda, *Angew. Chem.* **2011**, 123, 1641.
- [25] J. Patel, L. Němcová, P. Maguire, W. G. Graham, D. Mariotti, *Nanotechnology* **2013**, 24, 245604.
- [26] Q. Chen, T. Kaneko, R. Hatakeyama, *Appl. Phys. Express* **2012**, 5, 086201.
- [27] P. Rumbach, D. B. Go, *Top. Catal.* **2017**, 60, 799.
- [28] S. Pedireddy, H. K. Lee, W. W. Tjiu, I. Y. Phang, H. R. Tan, S. Q. Chua, C. Troadec, X. Y. Ling, *Nat. Commun.* **2014**, 5, 4947.
- [29] B. R. Panda, A. Chattopadhyay, *J. Nanosci. Nanotechnol.* **2007**, 7, 1911.
- [30] D. Wang, P. Schaaf, *J. Mater. Chem.* **2012**, 22, 5344.
- [31] A. Suker, L. P. H. Saravia, M. Bertotti, *Phys. Chem. Chem. Phys.* **2015**, 17, 28510.
- [32] A. Suker, M. Bertotti, *J. Braz. Chem. Soc.* **2017**.
- [33] H. Zheng, C. Picard, S. Ravaine, *Front. Chem. Sci. Eng.* **2018**, 12, 247.
- [34] Y. Gao, Y. Ding, *Chemistry* **2020**, 26, 8845.
- [35] J. A. Tapia Burgos, C. Mahr, A. R. S. Olaya, L. Robben, M. Schowalter, A. Rosenauer, G. Wittstock, A. Wittstock, M. Bäumer, *SSRN Electronic Journal* **2021**.
- [36] E. Artmann, P. V. Menezes, L. Forschner, M. M. Elnagar, L. A. Kibler, T. Jacob, A. K. Engstfeld, *ChemPhysChem* **2021**, 22, 2429.
- [37] S. K. Sengupta, *J. Electrochem. Soc.* **1998**, 145, 2209.
- [38] S. K. Sengupta, O. P. Singh, *J. Electroanal. Chem.* **1994**, 369, 113.
- [39] A. Hickling, M. D. Ingram, *Trans. Faraday Soc.* **1964**, p. 783–793.
- [40] E. Artmann, L. Forschner, T. Jacob, A. K. Engstfeld, *J. Vac. Sci. Technol. A* **2022**, 40, 053005.

- [41] A. Yerokhin, V. R. Mukaeva, E. V. Parfenov, N. Laugel, A. Matthews, *Electrochim. Acta* **2019**, *312*, 441.
- [42] J. J. Pireaux, M. Liehr, P. A. Thiry, J. P. Delrue, R. Caudano, *Surf. Sci.* **1984**, *141*, 221.
- [43] L. K. Ono, B. Roldan Cuenya, *J. Phys. Chem. C* **2008**, *112*, 4676.
- [44] E. Irissou, M.-C. Denis, M. Chaker, D. Guay, *Thin Solid Films* **2005**, *472*, 49.
- [45] M. P. Seah, G. C. Smith, M. T. Anthony, *Surf. Interface Anal.* **1990**, *15*, 293.
- [46] J. Szlachetko, J. Sá, M. Nachtegaal, U. Hartfelder, J.-C. Dousse, J. Hoszowska, D. L. Abreu Fernandes, H. Shi, C. Stampfl, *J. Phys. Chem. Lett.* **2014**, *5*, 80.
- [47] H. Shi, R. Asahi, C. Stampfl, *Phys. Rev. B* **2007**, *75*.
- [48] T. Dickinson, A. F. Povey, P. M. A. Sherwood, *J. Chem. Soc. Faraday Trans. 1* **1975**, *71*, 298.
- [49] A. Krozer, M. Rodahl, *J. Vac. Sci. Technol. A* **1997**, *15*, 1704.
- [50] N. Saliba, D. Parker, B. Koel, *Surf. Sci.* **1998**, *410*, 270.
- [51] A. Vitrey, R. Alvarez, A. Palmero, M. U. González, J. M. García-Martín, *Beilstein J. Nanotechnol.* **2017**, *8*, 434.
- [52] K. Azumi, T. Mizuno, T. Akimoto, T. Ohmori, *J. Electrochem. Soc.* **1999**, *146*, 3374.
- [53] H. H. Kellogg, *J. Electrochem. Soc.* **1950**, *97*, 133.
- [54] H. Tsai, E. Hu, K. Perng, M. Chen, J.-C. Wu, Y.-S. Chang, *Surf. Sci.* **2003**, *537*, L447.
- [55] A. L. Yerokhin, X. Nie, A. Leyland, A. Matthews, S. J. Dowey, *Surf. Coat. Technol.* **1999**, *122*, 73.
- [56] X. Jin, X. Wang, J. Yue, Y. Cai, H. Zhang, *Electrochim. Acta* **2010**, *56*, 925.
- [57] S. K. Sengupta, O. P. Singh, *J. Electroanal. Chem. Interfacial Electrochem.* **1991**, *301*, 189.
- [58] S. K. Sen Gupta, R. Singh, *Plasma Sources Sci. Technol.* **2017**, *26*, 015005.
- [59] G. Saito, Y. Nakasugi, T. Akiyama, *J. Appl. Phys.* **2015**, *118*, 023303.
- [60] P. Mandin, R. Wüthrich, H. Roustan, *AIChE J.* **2010**, *53*, 2446.
- [61] B. Zheng, K. Wang, M. Shrestha, T. Schuelke, Q. H. Fan, *Plasma Sources Sci. Technol.* **2019**, *28*, 085016.

Manuscript received: August 26, 2022

Revised manuscript received: October 27, 2022

Accepted manuscript online: November 3, 2022

Version of record online: December 2, 2022
